Journal of Zhejiang University-SCIENCE A (Applied Physics & Engineering)
ISSN 1673-565X (Print); ISSN 1862-1775 (Online)
www.jzus.zju.edu.cn; www.springerlink.com
E-mail: jzus@zju.edu.cn

Development of limestone calcined clay cement concrete in South China and its bond behavior with steel reinforcement*

Zhen-yu HUANG[1], You-shuo HUANG[1], Wen-yu LIAO[2], Ning-xu HAN[1], Ying-wu ZHOU[1], Feng XING[1], Tong-bo SUI[3], Bin WANG[3], Hong-yan MA[†‡2]

[1]*Guangdong Provincial Key Laboratory of Durability for Marine Civil Engineering, Shenzhen University, Shenzhen 518060, China*

[2]*Department of Civil, Architectural and Environmental Engineering, Missouri University of Science and Technology, Rolla, MO 65401, USA*

[3]*Sinoma Research Institute, Sinoma International Engineering Co., Ltd., Beijing 100102, China*

[†]E-mail: mahon@mst.edu

Received Apr. 10, 2020; Revision accepted June 16, 2020; Crosschecked Oct. 16, 2020

Abstract: Limestone calcined clay cement (LC^3), consisting of ordinary Portland cement (OPC) clinker, calcined clay, limestone powder, and gypsum, has been considered a promising solution to current challenges in the cement and concrete industry, such as high carbon emissions, high energy consumption, and resource shortages. This study carries out a series of experimental investigations of LC^3-based paste, mortar, and concrete, including microstructural analyses (e.g. hydration product characterization and pore structure analysis) and macro-scale testing (e.g. workability and mechanical properties), using raw materials from south China. The results show that, in LC^3 paste, the replacement of clinker by calcined clay and limestone leads to an increased volume of small pores but decreased total volume of pores. The workability of LC^3 mortar and concrete can be readily tailored using conventional superplasticizers. When designed for comparable 28-d compressive strength, the LC^3 mortar and concrete tend to have lower early-age compressive strength, but comparable compressive strength and higher flexural strength than those of the OPC counterparts at late ages. This study also examines the bond-slip behavior between LC^3 concrete and steel bars and finds that the bond strength is comparable to that of OPC concrete with the same 28-d compressive strength, but that the LC^3 concrete-rebar interface exhibits higher bond-slip stiffness. These findings on LC^3 concrete provide fundamental information and guidance for furthering the application of LC^3 binder in structural concrete in the near future.

Key words: Limestone calcined clay cement (LC^3); Hydration; Bond-slip; Mercury intrusion porosimetry (MIP); Scanning electron microscope (SEM); Bond strength

https://doi.org/10.1631/jzus.A2000163 **CLC number:** TU528.59

1 Introduction

With continuous world economic and population growth, the demand for civil infrastructure construction is increasing. Construction of this infrastructure relies heavily on concrete materials. To meet the increasing demand in infrastructure systems, production of cement has grown rapidly (Díaz et al., 2017), outstripping production of all other common infrastructure materials (Kelly and Matos, 2015). According to industry statistics (CEMBUREAU, 2015), global cement production is currently greater than 4.5 billion tons per year. However, cement production is an industrial process with high carbon emissions and high energy consumption. Carbon emissions from cement production are associated mainly with three aspects: (1) the grinding of raw materials into

‡ Corresponding author

* Project supported by the National Natural Science Foundation of China (Nos. 51708360 and 51978407), the Shenzhen Basic Research Project of China (No. JCYJ20180305124106675), the Key Projects for International Cooperation in Science, Technology and Innovation of China (No. 2018YFE0125000), the Taipei University of Technology-Shenzhen University Joint Research Program of China (No. 2020008), the National Science Foundation of the USA (No. 1661609), and the Advanced Materials for Sustainable Infrastructure Seed Funding Program at Missouri University of Science and Technology, USA

ORCID: Zhen-yu HUANG, https://orcid.org/0000-0002-8945-9445; Hong-yan MA, https://orcid.org/0000-0003-3674-3845

powders, which consumes a great amount of energy and releases CO_2, (2) the heating of raw materials in kilns to 1450 °C to form clinker, then co-grinding it with gypsum to make cement, and (3) process emissions (the decomposition of limestone releases CO_2). Overall, CO_2 emissions from cement production account for the largest proportion (52%) of industrial process-related CO_2 emissions (Edenhofer et al., 2014). If no changes are implemented, emissions of carbon dioxide, NO_x, particulate matter, and SO_2 linked to the cement production industry are likely to increase in the future, spurred by further economic development and urbanization.

In recent years, environmentally friendly (or eco-efficient) cement-based materials have been proposed and studied extensively. The replacement of cement by supplementary cementitious materials (SCMs) appears to be the most effective and economical way to achieve green goals in cementitious material development (Lothenbach et al., 2011; Scrivener et al., 2018a). Of all relevant strategies (also including alternative cements and cement efficiency improvement), SCMs have great potential to reduce carbon emissions and resource consumption in cement production. Typical SCMs include fly ash, slag, silica fume, and natural ashes (Alujas et al., 2015). Among them, fly ash and slag, which are widely used, have only global productions of around 15% of commercial cement production. This percentage will drop to less than 10% in the near future due to a shortage of quality materials (Damtoft et al., 2008; Schneider et al., 2011). Nevertheless, other available SCMs (e.g. silica fume, waste glass, natural pozzolans, and vegetable ashes) are limited by either their total production capacity or geographical/seasonal availability (Scrivener et al., 2018a). It will be a great challenge in the future to identify SCM resources that are abundant enough to meet the enormous demand from the cement and concrete industry. Fig. 1 summarizes the estimated availability of possible SCMs. Clay and limestone are apparently the solutions to address the future demand for SCMs, when simply considering quantity. Actual uses of clay and limestone as SCMs will also depend on logistics, exact chemical and mineralogical composition, contamination, and local availabilities (Scrivener et al., 2018a).

Limestone calcined clay cement (LC^3) is an emerging cement production strategy with a low clinker ratio and the partial replacement of clinker by calcined clay and limestone. Strictly speaking, LC^3 is a blended cement in which calcined clay and limestone are mixed and used as SCMs (Antoni et al., 2012). Since LC^3 utilizes only about 50% clinker, while clay is calcined under only 700–800 °C (instead of 1450 °C for clinker production), and limestone needs only grinding, LC^3 can effectively reduce carbon emission and energy consumption in cement production. In addition, production of LC^3 can directly utilize ordinary cement industry equipment and facilities, indicating a viable and relatively easy technology-to-market transition (Berriel et al., 2016). Thus, LC^3-based concrete has the potential to become a new, dominant green construction material (Antoni et al., 2012; Scrivener et al., 2018a). In the past few years, various aspects of LC^3-based materials have been investigated, including pozzolanic reactivity analysis of calcined clay (Tironi et al., 2012b; Alujas et al., 2015; Avet et al., 2016), overall hydration mechanisms of LC^3 (Antoni et al., 2012; Avet and Scrivener, 2018; Avet et al., 2018; Liao et al., 2019), rheological properties (Muzenda et al., 2020), microstructural development (Tironi et al., 2012a), durability and mechanical properties (Dhandapani et al., 2018), dimension stability (Ston and Scrivener, 2019), mixture proportioning methods (Scrivener and Favier, 2015), as well as life cycle assessment and the cost-efficiency of LC^3 (Berriel et al., 2016; Scrivener et al., 2018b).

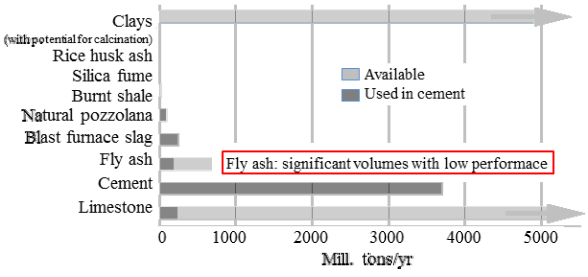

Fig. 1 Use and estimated availability of possible SCMs. Reprinted from Scrivener et al. (2018b), Copyright 2018, with permission from Elsevier

Antoni et al. (2012) investigated the combined effect of metakaolin and limestone added in cement. They examined the mechanical properties and microstructure of the modified mortars compared to ordinary Portland cement (OPC) mortar and found

that 45% substitution with a 2:1 blend of metakaolin (30%) and limestone (15%) resulted in better mechanical properties (Berriel et al., 2016; Avet et al., 2018). The mechanism of this enhancement was attributed to the reaction between the calcium carbonate from the limestone and the alumina from the metakaolin, forming supplementary AFm (alumina, ferric oxide, mono-sulfate) phases and stabilizing ettringite. Gmür et al. (2016) affirmed that calcined clays with aging conditions represented an attractive option as SCMs and featured robust properties against mechanisms of environmental deterioration. Their test results also confirmed that clays with moderate kaolinite content constituted a potential source of high pozzolanic reactivity. The compressive strength of the blended cement using 30% calcined clay with medium and high kaolinite content (above 40% kaolinite) yielded the same 28-d compressive strength level as plain OPC mortar. Similar results were also found by Avet et al. (2016) and Dhandapani et al. (2018): a comparable compressive strength and higher resistivity obtained by calcined clays with kaolinite content ≥40% at an age of 7 d compared to plain OPC mortars without extended curing. Porosimetry results showed a reduction of pore sizes in LC^3 as curing age increased. All these promising properties indicated the potential benefits of a LC^3 binder for the development of structural concrete, especially in a chloride-laden environment. These studies confirmed that kaolinite content was a significant factor governing the properties of LC^3. However, most previous studies only focused on the hydration mechanism and microstructure characterization of LC^3 pastes or mortars at the material level. There have been few investigations on the level of concrete technology and structural application. It is still not clear whether LC^3 can be used reliably and adaptively in reinforced concrete (RC) structures. For example, the excellent mechanical performance of RC structures relies significantly on the strong composite action between concrete and the steel rebar. Pull-out tests of steel rebar embedded in concrete are a frequently used test method to evaluate the interfacial bond behavior between these two materials (Hou et al., 2018; Zhou et al., 2019; Wang et al., 2020). Nevertheless, the interfacial bonding capacity of LC^3 concrete to steel rebar has not yet been studied. Several researchers have summarized recent needs in the research and development of LC^3 (Scrivener and Favier, 2015; Martirena et al., 2018). They suggested that further research priority should be given to the optimization of blends based on local raw materials, adapting the mix proportions of LC^3 concrete based on its application, and the enhancement (using LC^3) of durability of concrete structures where chloride resistance is important.

With the goal of addressing current research demands, this study aims to develop a LC^3 binder based on local (South China) raw materials, characterize its hydration behavior and microstructure development, and evaluate the workability and strength development properties of LC^3 concrete. Furthermore, the fundamental bond-slip behaviors between LC^3 concrete and steel rebar are investigated through pull-out tests, and the behavior is compared with that of OPC concrete of the same 28-d compressive strength.

2 Material development and methodology

2.1 Raw materials

The calcined clay used in this study was made from kaolin tailings calcined at 700–800 °C, which were collected from a trial industrial production carried out in Maoming, Guangdong Province, China. Fig. 2 shows the X-ray diffraction (XRD) patterns of raw kaolin tailings and calcined clay. The main phases of raw clay before calcining are quartz, kaolinite, illite, and a small amount of beidellite. After calcination, the sample contained quartz and illite, and the kaolinite was completely decomposed into amorphous metakaolin (indicated by the broad hump between 20° and 35°). Local OPC (P·I 52.5)

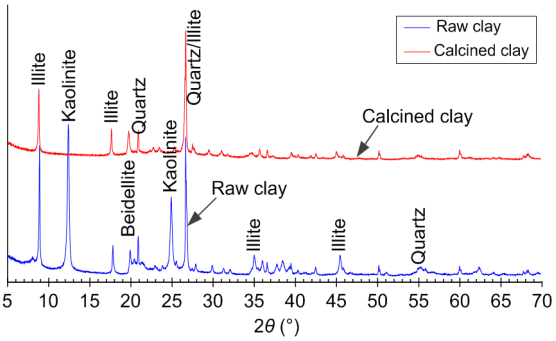

Fig. 2 XRD of the raw clay and calcined clay

conforming to GAQSIQ and SA (2007) was used. Previous work shows that a calcined clay-to-limestone ratio of 2:1 provided the best compressive strength development (Antoni et al., 2012; Scrivener et al., 2018b). Therefore, the LC^3 system was proportioned with 30% calcined clay, 15% limestone, and 55% OPC-gypsum mixture (in which extra gypsum was added to compensate for that in the OPC so as to achieve an overall gypsum content of 5%). The chemical compositions of the limestone, calcined clay, gypsum, and OPC used to prepare the LC^3 binder are presented in Table 1. Standard fine sand with a fineness of 2.67 was used to cast the mortar. For LC^3 concrete, a granite coarse aggregate with continuous grading and a maximum diameter of 20 mm was used. A high-water reducing agent, polycarboxylate-based superplasticizer (SP) was used to make a workable concrete. Steel rebars (HRB400 hot rolled bar) with diameters of 12 mm, 16 mm, and 20 mm were used for pull-out tests.

The particle size distributions of raw materials were measured by a laser particle analyzer. The results are presented in Fig. 3 and show that the median particle sizes of the calcined clay, OPC, and gypsum powder are 8.92 μm, 16.08 μm, and 25.97 μm, respectively. It is evident that the calcined clay is finer than OPC, which would affect pozzolanic activity, workability performance, and other important related properties. Limestone powders with three different degrees of fineness (S1, S2, and S3) were considered in the tests, as shown in Fig. 3b. The mean particle sizes were 47.4 μm, 30.2 μm, and 13.0 μm for S1, S2, and S3, respectively.

Table 1 Chemical composition of the raw materials

Oxide	Composition (%)			
	Calcined clay	Gypsum	Limestone	OPC
SiO_2	52.70	3.09	0.30	22.37
Al_2O_3	36.90	1.34	0.10	4.36
K_2O	3.49	0.05	–	–
Fe_2O_3	1.99	0.36	0.08	3.38
MgO	0.28	1.31	0.64	2.43
TiO_2	0.18	–	–	–
SO_3	0.12	40.87	–	2.45
CaO	0.04	30.51	81.13	61.08
Rb_2O	0.03	–	–	–
SrO	–	–	0.02	–
Others	4.27	23.26	17.73	2.71

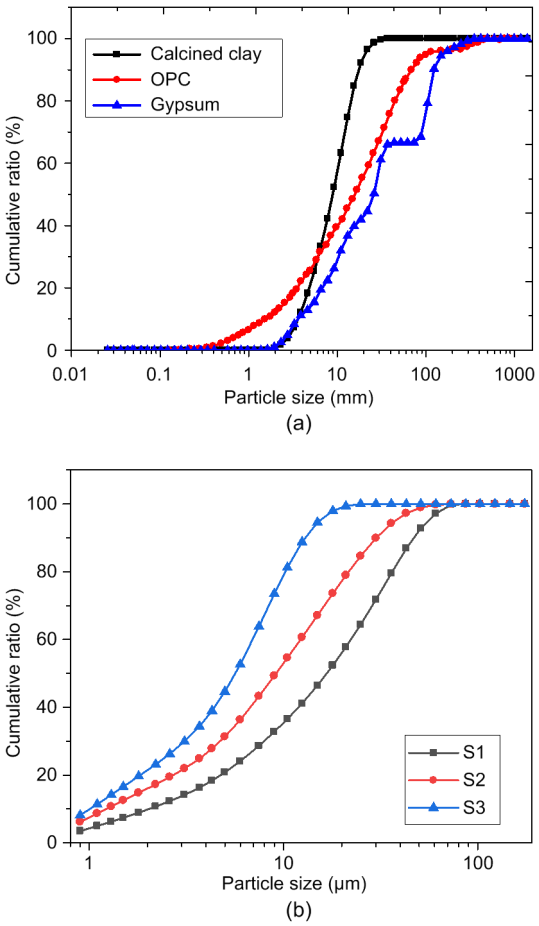

Fig. 3 Particle size distributions of raw materials
(a) Calcined clay, OPC, and gypsum; (b) Limestone

2.2 Mix proportions and specimen preparation

There were three types of materials considered in this study, namely, cement pastes, mortar, and concrete. Cement pastes were designed for microstructural analysis including scanning electron microscope (SEM), XRD, and mercury intrusion porosimetry (MIP) characterizations. Mortar specimens included 50 mm×50 mm×50 mm cubes and 40 mm×40 mm×160 mm prisms and were cast to determine the compressive and flexural strength developments of the OPC and LC^3 blends at different curing ages, according to SBQTS (1999) and ASTM (2010). As for concrete, 100 mm×100 mm×100 mm concrete cubes and 100 mm×100 mm×400 mm prisms were cast to explore the compressive, splitting, and flexural strengths according to Chinese code (MHURC, 2011). In addition, Standards of GAQSIQ and SA (2005) and ASTM (2009) were also used to measure

the flow value and slump of mortar and concrete, respectively, to evaluate their workability. To examine the bond behavior of rebar in the concrete specimens, this study adopted pull-out tests, which have been widely used in the literature (Hou et al., 2018; Zhou et al., 2019; Wang et al., 2020). Three groups of 150 mm ×150 mm×150 mm concrete substrate embedded with steel bars were prepared to investigate the bond-slip behavior between LC^3 concrete and steel rebar, in comparison with that between OPC concrete and steel rebar. Table 2 presents the binder system compositions of OPC and LC^3, while Table 3 presents the mix proportions of mortars and concretes. The raw materials were weighted carefully according to the mix proportions and put into a mandatory dual-shaft mixer. A 2-min dry stirring was implemented to ensure uniform mixing of the solid precursors, then water was slowly added, followed by the superplasticizer. The mortar fluidity and concrete workability were measured and recorded according to GAQSIQ and SA (2005) and ASTM (2009), respectively. For better comparison, the experiments adjusted similar flow and slump values for the OPC and LC^3 mixes by using the superplasticizer during casting. Given the particle size distribution curves in Fig. 3, it is evident that calcined clay is much finer than OPC, and so, with the same water-to-binder ratio (W/B), the LC^3 binder tends to be more viscous than OPC. Therefore, more superplasticizer is needed to achieve workability comparable to OPC. Table 3 shows that comparable flowability of mortar and/or slump of concrete can be achieved by adjusting the content of superplasticizer. Fig. 4 shows the flows and slumps of the OPC and LC^3 mortar and concrete. Specimens prepared with various dimensions were demolded after 24 h and cured in a standard fog room with temperatures of (20±2) °C and a relative humidity of >95%.

The pull-out test specimens were divided into an OPC group (a control group) and an LC^3 group (Table 4). The variables under investigation include different binders, water-to-binder ratios, and rebar diameters. The W/B reflects different levels of compressive strength. The W/B of the control group was 0.4, while a range of W/B values of 0.30, 0.35, and 0.40 were considered in the LC^3 concrete group. During specimen preparation, the steel bar was placed horizontally in a wooden mold and a 50-mm long polyvinyl chloride (PVC) tube was set at the loading end and the free end to form unbound regions so as to reduce the effect of stress concentration (Zhou et al., 2019). HRB400 deformed rebar, which is commonly used in structural design practice, was adopted in this study, and the embedded length of the rebar in concrete kept consistent at 50 mm. The specific dimension and detailing of the specimen are shown in Fig. 5b.

Table 2 Binder system compositions

Binder	Proportion (%)				W/B
	Cement	CC	LS	GYP	
OPC	100.0	0.0	0.0	0.0	0.50
LC^3	52.3	30.0	15.0	2.7	0.50

CC: calcined clay; LS: limestone powder; GYP: gypsum powder

Table 3 Mix proportion of mortar and concrete

Mixture No.	W/B	Binder proportion				Proportion			Slump/flow (mm)	Remark
		OPC	CC	LS	GYP	Sand	CAgg	SP		
OPM-0.50	0.50	1.000	−	−	−	3.00	−	−	230	OPC mortar
OPM-0.45	0.45	1.000	−	−	−	3.00	−	−	200	
OPM-0.40	0.40	1.000	−	−	−	3.00	−	0.0027	190	
OPM-0.35	0.35	1.000	−	−	−	3.00	−	0.0047	185	
LCM-0.50	0.50	0.523	0.300	0.150	0.027	3.00	−	0.0037	220	LC^3 mortar
LCM-0.45	0.45	0.523	0.300	0.150	0.027	3.00	−	0.0052	200	
LCM-0.40	0.40	0.523	0.300	0.150	0.027	3.00	−	0.0073	180	
LCM-0.35	0.35	0.523	0.300	0.150	0.027	3.00	−	0.0115	180	
OC-0.50	0.50	1.000	−	−	−	1.43	2.21	–	190	OPC concrete
OC-0.40	0.40	1.000	−	−	−	1.43	2.21	0.0032	70	
LCC-0.50	0.50	0.523	0.300	0.150	0.027	1.43	2.21	0.0032	175	LC^3 concrete
LCC-0.40	0.40	0.523	0.300	0.150	0.027	1.43	2.21	0.0057	90	

CAgg: coarse aggregate; SP: superplasticizer. OPM: OPC mortar; LCM: LC^3 mortar; OC: OPC concrete; LCC: LC^3 concrete

Table 4 Pull-out test plan

Specimen No.	Binder	W/B	f_c (MPa)	d (mm)	f_y (MPa)	L (mm)
PNC	OPC	0.40	59	16	395	50
PLC3	LC^3	0.40	54.6	16	395	50
PLC3-D12	LC^3	0.40	54.6	12	436	50
PLC3-D22	LC^3	0.40	54.6	22	345	50
PLC3-0.35	PLC3-1	0.35	59	16	395	50
PLC3-0.30	PLC3-1	0.30	78.1	16	395	50

f_c: compressive strength; d: rebar diameter; f_y: yield strength; L: embedded length of rebar in concrete

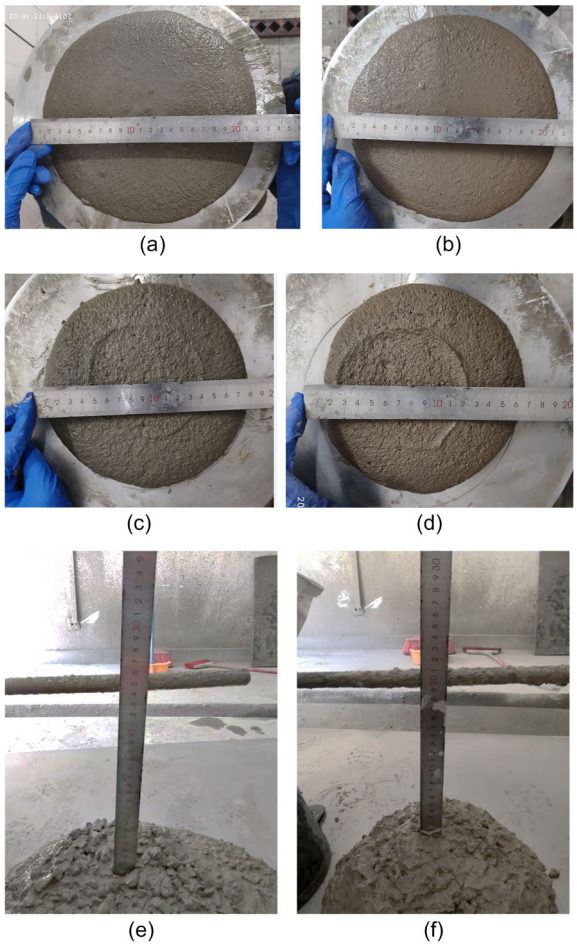

Fig. 4 Flow and slump tests of OPC and LC^3 mortar and concrete: (a) OPM-0.50; (b) LCM-0.50; (c) OPM-0.35; (d) LCM-0.35; (e) OC-0.50; (f) LCC-0.50

2.3 Test methods

The pastes were cured for 1 d, 3 d, 7 d, and 28 d, respectively, before samples were taken, and put into anhydrous ethanol for the termination of hydration reactions. After the termination of hydration, the samples were dried in a vacuum oven with a temperature of 60 °C. Following this, the dried samples were

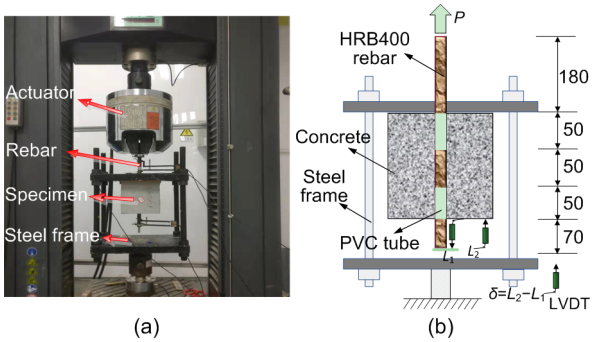

Fig. 5 Test setup and instrumentations for pull-out tests
(a) Test setup; (b) Dimensions and instrumentation (unit: mm). P: applied load; L_1: displacement of rebar end; L_2: displacement of concrete; δ: slip of rebar; LVDT: linear variable differential transformer

used for XRD, SEM, and MIP testing. XRD tests were conducted using a Bruker D8 Advance system. The samples were ground into powder form, and XRD scanning was conducted in the 2θ range of 7°−30° with a step size of 0.02° and a scanning rate of 0.1 (°)/s. SEM observations were implemented using a Quanta TM 250 FEG equipped with a field emission environmental scanning mirror. The samples were taken from the central part of damaged pieces of paste. Before scanning, the surfaces of the samples were treated with a gold coating. MIP tests were conducted using a Micromeritics AutoPore IV 9500 following the general instructions for experimental parameter selection and data processing (Ma, 2014).

The compressive, splitting, and flexural strength tests of mortar and concrete were carried out using a 200-t electro-hydraulic servo pressure testing machine with loading speeds of 0.5 MPa/s, 550 N/s, and 65 N/s (20 N/s for mortar), respectively. Before loading, the specimen surfaces were dried under indoor conditions. Table 5 lists the test methods and related testing standards used in this study. For each mechanical test, at least three specimens were tested.

Table 5 Test method references and specimen sizes

Property	Test standard	Testing age	Specimen type and size (mm)	Test number
Workability (flow value or slump)	Mortar: GAQSIQ and SA (2005); concrete: ASTM (2009)	Right after mixing	–	1
Compressive strength	Mortar: SBQTS (1999); concrete: MHURC (2011)	1, 3, 7, and 28 d	Cube: 50×50×50; cube: 100×100×100	3; 3
Flexural strength	Mortar: ASTM (2010); concrete: MHURC (2011)	1, 3, 7, and 28 d	Prism: 40×40×160; prism: 100×100×160	3; 3
Spitting strength	MHURC (2011)	1, 3, 7, and 28 d	Cube: 100×100×100	3
Bond-slip behavior	Hou et al. (2018); Zhou et al. (2019); Wang et al. (2020)	28 d	Cube: 150×150×150	3

The pull-out tests were carried out on a 300-kN Mechanical Testing & Simulation (MTS) machine in displacement control mode with a loading speed of 0.5 mm/min. The relative slip between rebar and concrete was measured using an extensometer, while the tensile strain of rebar was recorded by strain gauge. The slippage measured was the pure displacement of the steel bar relative to the top of the concrete substrate. Figs. 5a and 5b show details of the test setup and instrumentation. PVC tube was used to (1) ensure a more uniform shear stress distribution along the embedded length of the steel bar in concrete, and to (2) adjust the exact embedded length of the steel bar in concrete. Because directly embedding rebar in concrete may result in the largest bond stress in the loading end and the lowest stress in the bottom end, following an exponential function, the uniform bond stress assumption could not be applicable. Using PVC tube at the loading end and bottom end could address this problem. In this case, the average bond stress was assumed to be uniformly distributed along the contact area between the steel bar and the concrete. Eq. (1) can thus be used to calculate the average bond stress τ between the steel bar and concrete:

$$\tau=\frac{P}{\pi dl}, \tag{1}$$

where d is the rebar diameter, and l is the embedded length of steel bar. Thus, the bond strength can be calculated from the peak load.

3 Test result

3.1 Paste composition and microstructure

3.1.1 Hydration products

Fig. 6 shows and compares the XRD intensities of hydration products of OPC and LC^3 pastes with different curing ages. This figure reflects the difference in hydration mechanisms of LC^3 and OPC binders. Compared with OPC, the main hydration product observed in LC^3 paste are ettringite (E) and hemicarboaluminate (HC), apart from C-S-H. The peaks shown in Fig. 6 indicate that the calcium hydroxide (CH) in OPC observed is much higher than that in LC^3 binder, partially due to the 50% lower clinker content in LC^3. Another contributor to the weak peak of CH in LC^3 paste is that the secondary hydrations (Scrivener and Favier, 2015; Nidheesh and Kumar, 2019; Ston and Scrivener, 2019) as shown in Eqs. (2) and (3) (Matschei et al., 2007; Lothenbach et al., 2008; Damidot et al., 2011) consume CH. Apart from amorphous silica that reacts with CH, the aluminum phase in calcined clay (when coupled with limestone) also reacts with CH to form calcium carboaluminate hydrate. The peaks of calcium carbonate and quartz are believed to be leftovers from the limestone and calcined clay, respectively.

$$\mathrm{S+CH\rightarrow C\text{-}S\text{-}H}, \tag{2}$$

$$\mathrm{A_{(from\ calcined\ clay)}+C\bar{C}+3CH\rightarrow C_3A\cdot C\bar{C}\cdot H_{11}}, \tag{3}$$

where S represents amorphous silica from calcined clay, A represents alumina, C_3A represents tricalcium aluminate, and $C\bar{C}$ represents $CaCO_3$.

3.1.2 Morphology

SEM was conducted to observe the microscopic morphology of the hydration products of both OPC and LC^3 pastes. Figs. 7a–7f show the SEM images of OPC and LC^3 pastes with a W/B of 0.50 and curing ages of 1, 3, and 28 d. It can be seen from the SEM images that the main hydration products of OPC contain CH with thin hexagonal flakes (Fig. 7b),

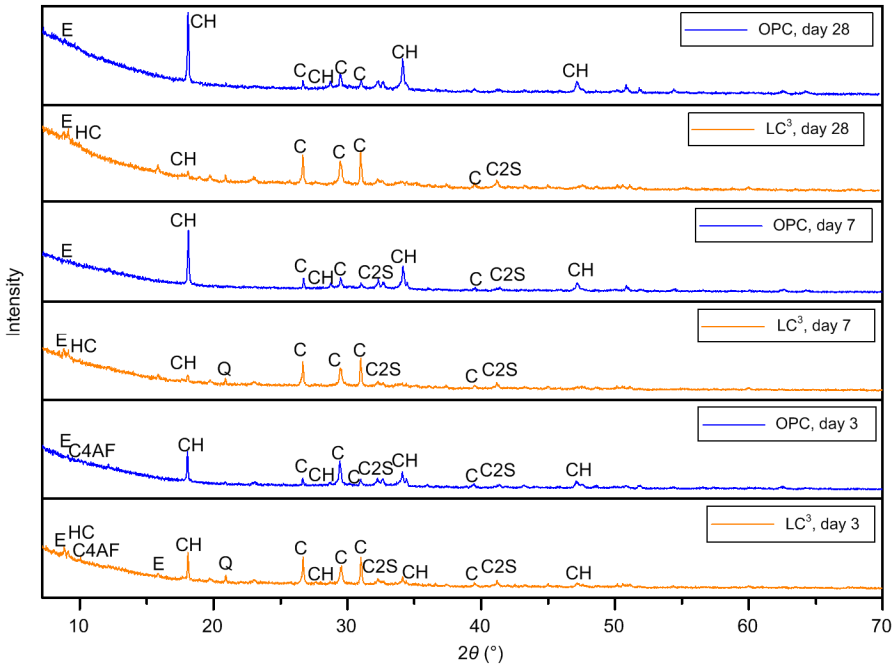

Fig. 6 XRD plots of OPC and LC^3 pastes with different curing ages
C: tricalcium silicate; C2S: dicalcium silicate; C4AF: tetracalcium aluminoferrite; Q: quartz

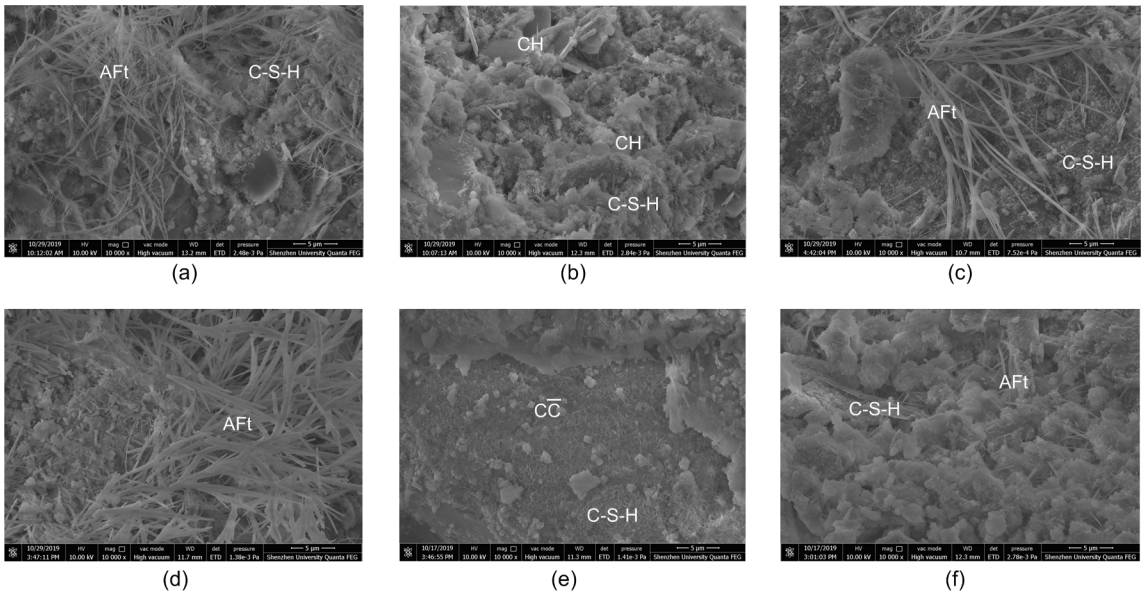

Fig. 7 SEM images of OPC and LC^3 pastes under different curing ages: (a) LC^3, day 1; (b) OPC, day 1; (c) LC^3, day 3; (d) OPC, day 3; (e) LC^3, day 28; (f) OPC, day 28 (AFt indicates alumino, ferrous, tri-sulfate, or ettringite)

relatively dense netlike C-(A)-S-H gel (Figs. 7b and 7f), and the acicular substance ettringite (Figs. 7d and 7f) with a length greater than 10 μm (Antoni et al., 2012). Compared to the OPC paste, the hydration products in the LC^3 system contain smaller amounts of CH crystals, and the contents of carboaluminate and calcium carbonate (Figs. 7a, 7c, and 7e) appear to be relatively high, which matches the XRD results.

3.1.3 Pore size analysis

Because porosity is directly tied to the density and strength of the binder system, the pore structure

analysis of OPC and LC^3 pastes is an important step in revealing the relationship between the microstructure and mechanical properties of LC^3 concrete. Through MIP, the pore size distribution of the pastes with different W/B values at different curing ages can be obtained. Fig. 8 shows the cumulative pore volume curves of OPC and LC^3 pastes. After 3 d of curing time, the total pore volume of the LC^3 paste is higher than that of OPC. This can be attributed to slow pozzolanic reactions at earlier ages due to the overall low alkalinity. However, because of the pozzolanic reactions of calcined clay as discussed in Section 3.1.1, at the late age of 28 d the LC^3 paste achieves a lower porosity as well as a finer pore structure (Antoni et al., 2012; Avet et al., 2016; Avet and Scrivener, 2018). These pore structure features also indicate that LC^3 could obtain comparable or even higher long-term compressive strength as well as superior impermeability compared to that of OPC paste with the same W/B (Ma and Li, 2013a; Ma et al., 2015). This finding is consistent with previous study (Alujas et al., 2015).

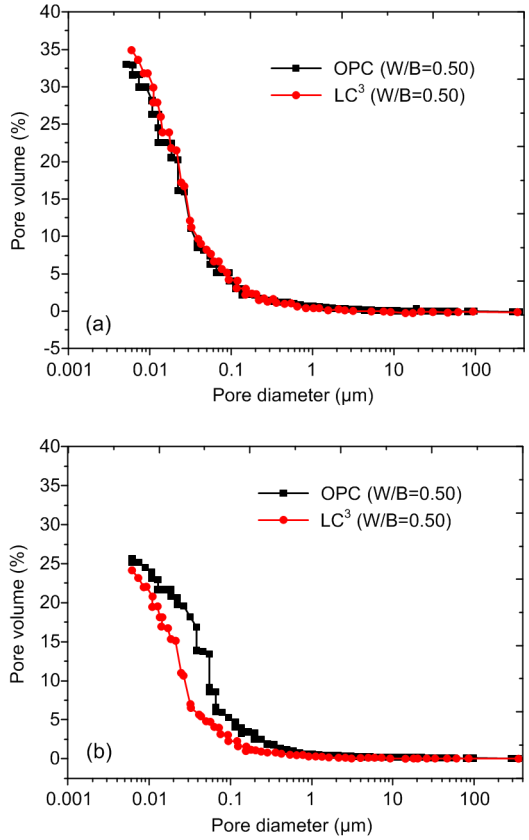

Fig. 8 Cumulative pore volume curves of OPC and LC^3 pastes: (a) day 3; (b) day 28

3.2 Mechanical properties

3.2.1 Compressive and flexural strengths of mortars

Fig. 9 shows the compressive and flexural strengths of LC^3 and OPC mortars with a W/B of 0.50. Note that the compressive strength of LC^3 mortar is lower than that of OPC mortar at early ages (i.e. 1 d and 3 d). After curing for 7 d, the compressive strength of LC^3 mortar achieves comparable strength or even exceeds that of OPC mortar. Flexural strength shows an increasing trend similar to compressive strength as shown in Fig. 9b. This is because of the secondary hydration reactions in LC^3 paste: (1) amorphous silica in calcined clay reacts with CH from cement hydration products to form C-S-H gel; (2) the alumina phase in the calcined clay reacts with limestone and CH to form calcium carbonaluminate hydrates, which fill the pores and make the microstructure more compact. It is worth noting that these reactions will not be initiated until the alkalinity of the

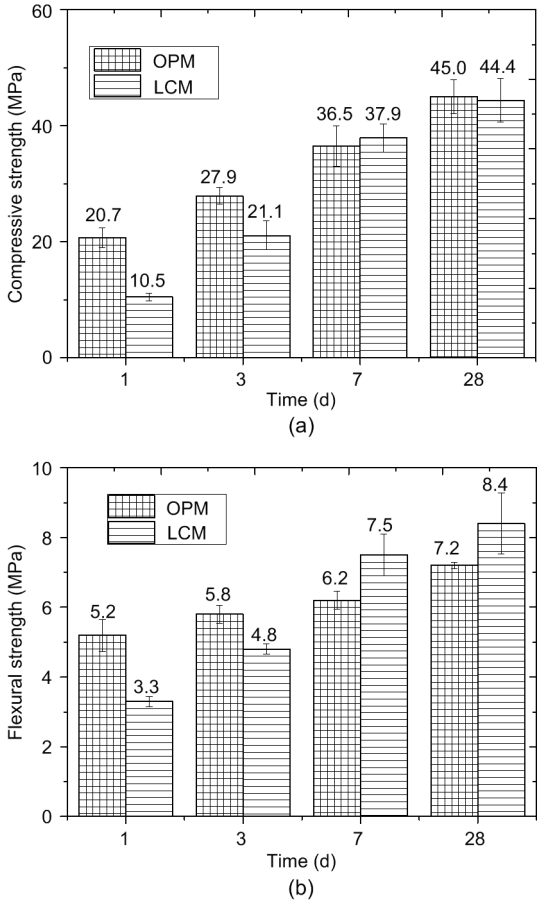

Fig. 9 Compressive (a) and flexural (b) strengths of OPC and LC^3 mortars with W/B=0.50

pore solution is high enough, likely after 3 d. The observed trends are consistent with the evolutions of pore structures described in Section 3.1.3. The results indicate that LC^3 can achieve comparable strength with less clinker compared to OPC. More importantly, given comparable compressive strengths at late ages, the flexural strength of LC^3 mortar is remarkably higher (i.e. 17% at 28 d) than that of OPC mortar. Since the flexural-to-compressive strength ratio is an index of toughness (Ma and Li, 2013b), LC^3-based materials are potentially tougher than OPC-based materials.

3.2.2 Effect of water-to-binder ratio

The W/B plays a significant role in strength development, which is a key parameter in concrete mix proportion design. Figs. 10a and 10b show the influence of W/B on the compressive and flexural strength development of LC^3 mortars. Note that the 28-d compressive and flexural strengths all increase with the decrease of W/B. With a low W/B of 0.35, LC^3 mortar can achieve a high compressive strength of 60.7 MPa and flexural strength of 10.7 MPa at the age of 28 d.

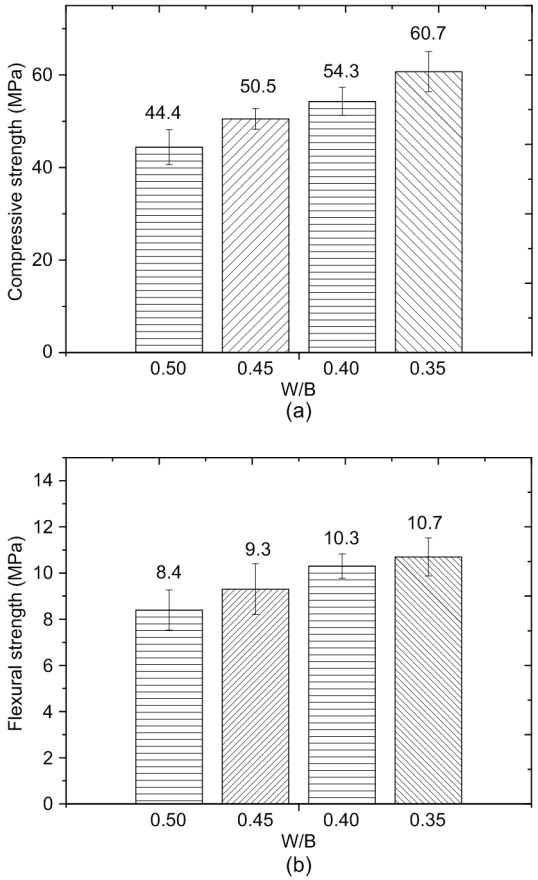

Fig. 10 Effect of W/B on 28-d compressive (a) and flexural (b) strength development of LC^3 mortar

3.2.3 Effect of fineness of limestone

Limestone powder in the LC^3 binder system has two functions—that of a filler and that of a reactant of secondary hydration. The fineness of limestone may affect both the filler effect and the rate of pozzolanic reaction. Normally, finer particles can result in higher reaction rates and accelerate early-age strength development. However, a high fineness could increase the water demand and adversely affect the workability and thus the compaction of fresh mortar. A poor compaction would compromise the compressive strength. This section selects three different finenesses of limestone (D_{50}=47.4 μm, 30.2 μm, and 13.0 μm) for strength comparison with a constant W/B of 0.50. Their corresponding specific surface areas are 4816 cm^2/g, 7285 cm^2/g, and 9414 cm^2/g. Figs. 11a and 11b show the compressive and flexural strengths of LC^3 mortar prepared with a different fineness of limestone, compared with that of OPC mortar. According to Fig. 11, prior to 3 d of curing, the compressive strength (f_c) of LC^3 mortars follows $f_{c,S2}>f_{c,S3}>f_{c,S1}$, whereas after 28 d of curing, the compressive strength follows $f_{c,S1}>f_{c,S2}>f_{c,S3}$. Similarly, the flexural strength (f_f) follows $f_{f,S2}>f_{f,S3}>f_{f,S1}$ before 3 d of curing, whereas it follows $f_{f,S1}>f_{f,S2}>f_{f,S3}$ after 7 d of curing. The results show that reasonably improving the fineness of limestone powder can improve the early-age strength of LC^3 mortar; however, it does not necessarily lead to superior long-term strength. Furthermore, if the fineness is too high, it could even harm early-age strength. In the cases with a W/B of 0.50, the LC^3 mixture using limestone with S1 (D_{50}=47.4 μm) achieves the highest 28-d compressive and flexural strengths. It seems that higher fineness tends to negatively influence the mechanical properties. Nevertheless, this conclusion should be limited to the W/B of 0.50. Whether this conclusion can be transplanted to other W/B needs to be determined in further research.

3.2.4 Compressive and tensile strengths of concrete

The previous sections evaluated the strengths of LC^3 and OPC mortars, showing the promising

workability and mechanical properties of LC^3. This section aims to evaluate the mechanical behaviors of LC^3 concrete, in order to promote its future applications as a structural material. It should be noted that all the specimens for compressive strength and splitting tests were cured in the same standard conditions with temperatures of (20±2) °C and a relative humidity of >95%. The test selected two W/B values of 0.40 and 0.50 for comparison. As the W/B increased, the compressive strengths of both LC^3 and OPC concretes decreased. With a W/B of 0.50, the compressive strength of LC^3 concrete could not match that of OPC concrete until the age of 28 d. The 28-d compressive strength of LC^3 concrete is slightly lower than that of OPC concrete, as shown in Fig. 12a. However, the LC^3 concrete has a higher rate of development at late ages, and it can be expected that its strength will match that of OPC concrete soon after 28 d. With a W/B of 0.40, the compressive strength of LC^3 concrete exceeds that of OPC

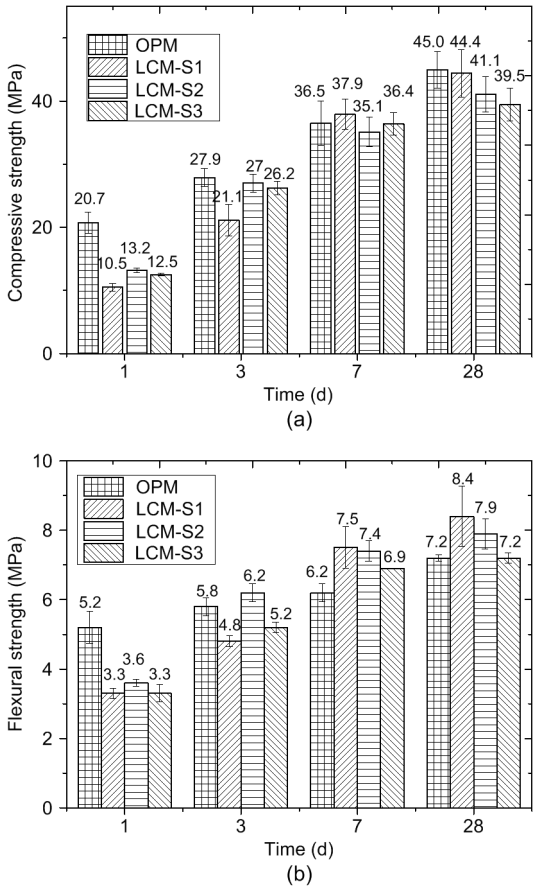

Fig. 11 Effect of fineness of limestone on compressive (a) and flexural (b) strengths

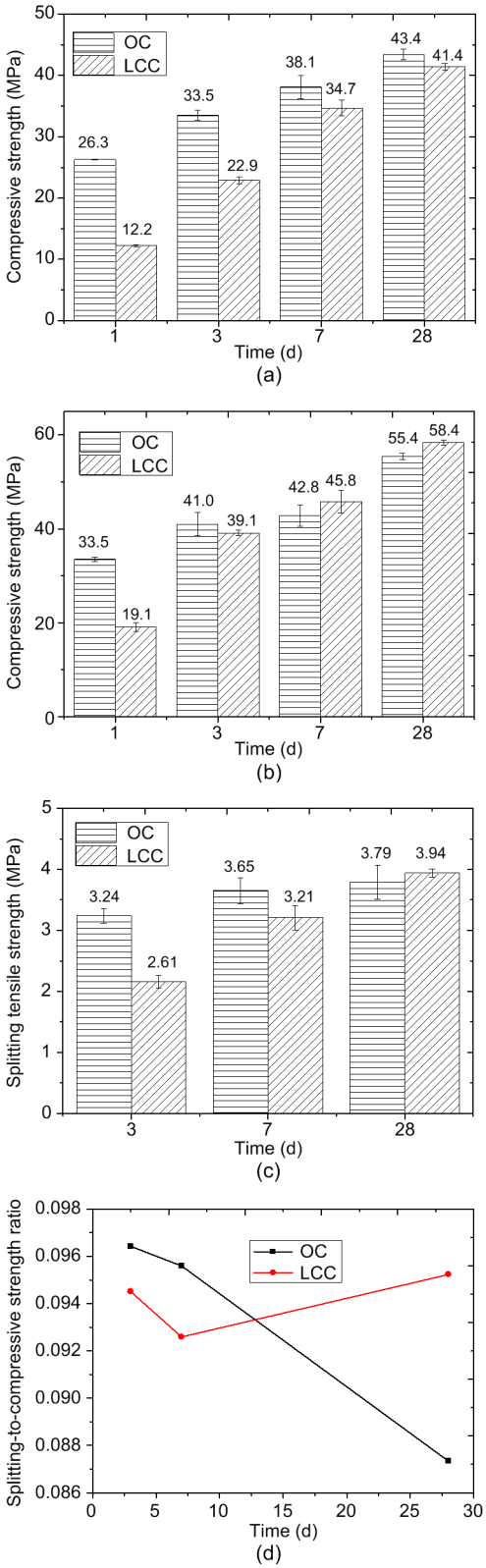

Fig. 12 Compressive and tensile strengths of concrete: (a) compressive strength with W/B=0.50; (b) compressive strength with W/B=0.40; (c) splitting tensile strength with W/B=0.50; (d) splitting-to-compressive strength ratio

concrete after 7 d of curing, as shown in Fig. 12b. These trends in both W/B values are consistent with that in mortars, and thus can be explained based on the theories laid out in Section 3.2.1. Moreover, the splitting tensile strength of LC^3 concrete (W/B=0.50) is lower than that of OPC concrete at early ages, and slightly higher than that of OPC at 28 d, as shown in Fig. 12c. When compared with Fig. 12a, it can be clearly seen that, though lower at early ages, the splitting-to-compressive strength ratio of LCC is higher at late age of 28 d, as confirmed in Fig. 12d. This suggests that the increasing rate of splitting tensile strength is higher than that of compressive strength in LC^3 concrete with an increase in curing age. Since a higher splitting-to-compressive strength ratio also indicates a higher toughness, this finding further confirms the conclusion of Section 3.2.1, namely, that LC^3-based materials are potentially tougher than the OPC-based materials.

3.3 Bond-slip relationship

3.3.1 Bond-slip curves

When a new binder is to be applied in reinforced concrete structures, an understanding of the composite action between concrete and rebar is of significant importance. A common method to assess this behavior is to use pull-out tests in which a rebar is pulled out from the concrete substrate in which the rebar was embedded. Based on the pull-out test results, the results of peak force, bond stress, ultimate bond strength corresponding to the slip between concrete and rebar, and failure modes can be obtained. Table 6 summarizes the test data of the pull-out tests.

Table 6 Data and failure modes of pull-out test

Specimen No.	f_c (MPa)	P_p (kN)	τ_u (MPa)	Failure mode
PNC	59.0	79.49	31.63	Pull-out
PLC3	54.6	73.24	29.14	Pull-out
PLC3-D22	54.6	92.30	26.71	Splitting
PLC3-D12	54.6	54.66	29.89	Pull-out
PLC3-0.35	59.0	81.25	32.33	Pull-out
PLC3-0.30	78.1	91.94	36.58	Pull-out

P_p: peak load in pull-out test; τ_u: ultimate bond strength

As shown in Table 6 and Fig. 13a, with the same rebar diameter (i.e. d=16 mm), the ultimate bond strength between LC^3 concrete and rebar increases linearly with the increase of the concrete compressive strength. The peak bond stresses of specimens with W/B values of 0.40, 0.35, and 0.30 achieve 29.14 MPa, 32.33 MPa, and 36.58 MPa, respectively. The initial stiffnesses of the bond stress-slip curves with different compressive strengths in the LC^3 group are very close. However, for the same compressive strength of OPC and LC^3 concretes, the initial stiffness of the OPC group is much lower than that of the LC^3 group. It may be due to a denser microstructure with less porosity and higher splitting-to-compressive strength ratio of LC^3 concrete compared to the OPC group, leading to a higher elastic modulus of concrete and enhanced bond stress between the concrete and the steel bar. Fig. 13b shows the bond stress-slip curves with different rebar diameters of 12 mm, 16 mm, and 22 mm, respectively. The bond stress-slip curves of PLC3–D12 and PLC3 are quite similar, whereas PLC3–D22 with a larger rebar diameter exhibits a sharp drop in bond stress. This reflects a different failure mode which is discussed in Section 3.3.2.

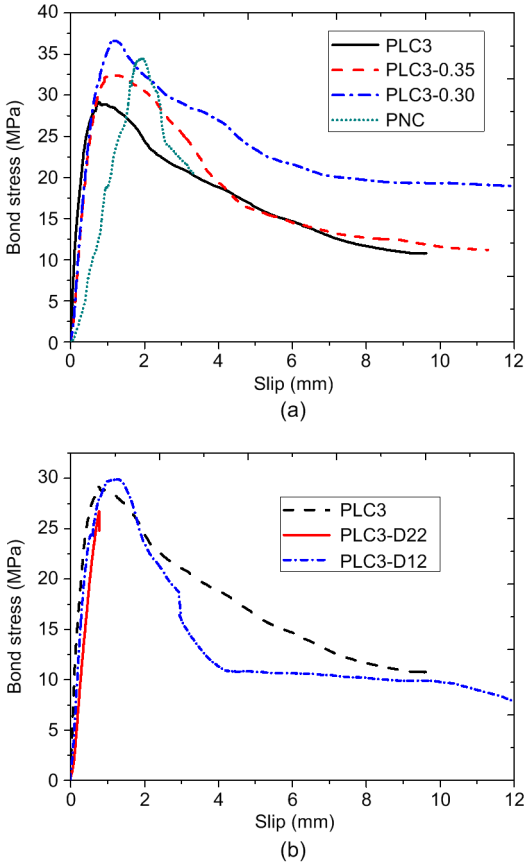

Fig. 13 Bond-slip curves of LC^3 and OPC concretes embedded with rebars: (a) effect of compressive strength; (b) effect of rebar diameter

3.3.2 Failure mode

As shown in Table 6 and Fig. 14, the specimen with a larger rebar diameter (d=22 mm) failed through concrete splitting, due to brittleness, whereas other specimens with smaller rebar diameters failed by pull-out failure of the rebar. The failure mode seems to be unrelated to the binder type but correlated to concrete strength and concrete cover. The general bond-slip behavior of the LC^3 group is similar to that of the OPC group. Fig. 13b shows that the peak bond stresses of the specimens with rebar diameters of 12 mm and 16 mm are approximately close. The rebar was pulled out from the concrete substrate, as shown in Figs. 14a and 14b. No macroscopic cracks appeared on the concrete surface. However, concrete splitting failure occurred in the specimen with rebar diameter of 22 mm. This was due to the relatively thinner concrete cover as the rebar diameter increased. During the pulling out of the rebar, the concrete around the rebar has insufficient tensile strength to resist the driving force. When the circumferential stress exceeds the tensile strength of the concrete, concrete cracks occur and propagate promptly along the length of the specimen, leading to splitting of the concrete substrate. At this point, the rebar rib profile inside the concrete surface is still clearly visible, as shown in Fig. 14d. This indicates that the bond strength related to this failure is contributed by the mechanical interaction between concrete and rebar, rather than friction interaction, and the bond strength has not reached its maximum value. Overall, the failure modes of specimens match the corresponding bond-slip curves presented in Fig. 13.

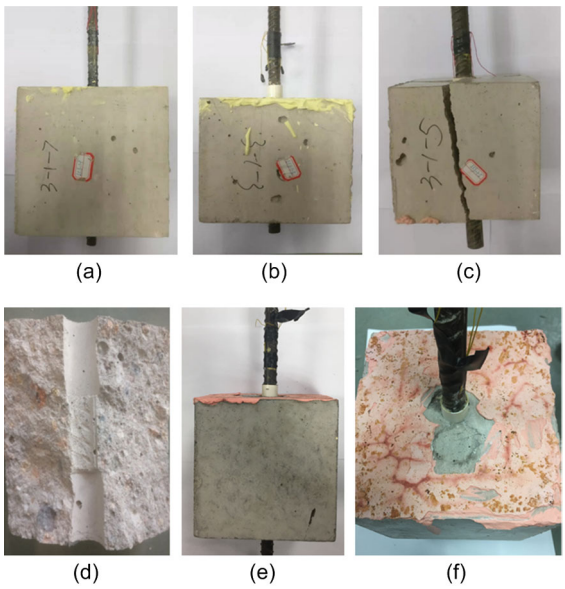

Fig. 14 Failure modes of the pull-out tests: (a) PLC3-D12 (d=12 mm, pull-out failure); (b) PLC3 (d=16 mm, pull-out failure); (c) PLC3-D22 (d=22 mm, concrete splitting failure); (d) failure profile in PLC3-D22; (e) OPC group; (f) pull-out rebar

4 Conclusions

The objective of this study was to investigate several fundamental problems of LC^3 paste, mortar, and concrete in the light of microscopic and macroscopic experiments. High-resolution XRD, SEM, and MIP were conducted to analyze the crystal phases, microscopic morphology, and pore structure of LC^3 paste in comparison with OPC paste. This study also produced LC^3 mortar and concrete, and evaluated their workability and mechanical performance. Finally, the interfacial bond behavior between LC^3 concrete and rebar, which reflects the composite action between these two materials and is a key performance in concrete structures, was studied. Based on this study, the following conclusions are suggested:

1. Compared with OPC, ettringite, monocarbonaluminate (MC), and HC are the main crystal hydration products in LC^3 samples. There is little hexagonal thin flake CH left in the hydration products of LC^3 because of 50% less clinker and because of the secondary hydration reactions occurring in LC^3 which consume a great amount of CH generated from the hydration of OPC clinker.

2. Compared with OPC mortar and concrete, the early strengths of LC^3 mortar and concrete are lower, whereas the late strength (after 7 d) increases rapidly to similar levels due to the secondary reactions of amorphous silica and alumina (coupled with limestone) in calcined clay, forming C-S-H and calcium carbonaluminate hydrates.

3. Given comparable compressive strengths, LC^3-based materials tend to have higher flexural or splitting tensile strength and are thus potentially tougher than their OPC counterparts.

4. In LC^3-based materials, a finer limestone does not necessarily result in higher performance.

5. Regarding the interfacial bond-slip behavior between LC^3 concrete and rebar, the failure mode is generally identical to that of the OPC group. Typically, two failure modes, namely, pull-out of rebar from the concrete substrate and concrete splitting, were observed in the tests. Given the same grade of compressive strength, the bond strength of LC^3 concrete is comparable to that of OPC concrete; however, the bond-slip stiffness of LC^3 concrete is greater than that of OPC counterpart.

To summarize, the fundamental findings of this study show that LC^3 concrete can be feasibly used in structural concrete design, especially for marine concrete structures, since LC^3 concrete exhibits denser microstructure, leading to better durability performance. It is even potentially tougher than OPC concrete. However, there is a need for more large-scaled experimental tests on LC^3 concrete structures, e.g. beams, columns, plates, and joints for structural evaluation. These preliminary conclusions need to be further tested in higher fidelity in future research.

Contributors

Zhen-yu HUANG designed the research plan and drafted the manuscript. You-shuo HUANG conducted the tests. Wen-yu LIAO processed the test data and edited the final version. Ning-xu HAN, Ying-wu ZHOU, and Feng XING contributed to methodology and organized the manuscript. Tong-bo SUI and Bin WANG provided the raw material data and helped to draft the test program. Hong-yan MA conceptualized and supervised the research, and finalized the manuscript.

Conflict of interest

Zhen-yu HUANG, You-shuo HUANG, Wen-yu LIAO, Ning-xu HAN, Ying-wu ZHOU, Feng XING, Tong-bo SUI, Bin WANG, and Hong-yan MA declare that they have no conflict of interest.

References

Alujas A, Fernández R, Quintana R, et al., 2015. Pozzolanic reactivity of low grade kaolinitic clays: influence of calcination temperature and impact of calcination products on OPC hydration. *Applied Clay Science*, 108:94-101. https://doi.org/10.1016/j.clay.2015.01.028

Antoni M, Rossen J, Martirena F, et al., 2012. Cement substitution by a combination of metakaolin and limestone. *Cement and Concrete Research*, 42(12):1579-1589. https://doi.org/10.1016/j.cemconres.2012.09.006

ASTM (American Society of Testing and Materials), 2009. Standard Test Method for Flow of Freshly Mixed Hydraulic Cement Concrete, C1362-09. National Standards of USA.

ASTM (American Society of Testing and Materials), 2010. Standard Test Method for Flexural Strength of Concrete (Using Simple Beam with Center-point Loading), C293-2010. National Standards of USA.

Avet F, Scrivener K, 2018. Investigation of the calcined kaolinite content on the hydration of limestone calcined clay cement (LC^3). *Cement and Concrete Research*, 107:124-135. https://doi.org/10.1016/j.cemconres.2018.02.016

Avet F, Snellings R, Alujas Diaz A, et al., 2016. Development of a new rapid, relevant and reliable (R^3) test method to evaluate the pozzolanic reactivity of calcined kaolinitic clays. *Cement and Concrete Research*, 85:1-11. https://doi.org/10.1016/j.cemconres.2016.02.015

Avet F, Li XR, Scrivener K, 2018. Determination of the amount of reacted metakaolin in calcined clay blends. *Cement and Concrete Research*, 106:40-48. https://doi.org/10.1016/j.cemconres.2018.01.009

Berriel SS, Favier A, Rosa Domínguez ER, et al., 2016. Assessing the environmental and economic potential of limestone calcined clay cement in Cuba. *Journal of Cleaner Production*, 124:361-369. https://doi.org/10.1016/j.jclepro.2016.02.125

CEMBUREAU (The European Cement Association), 2015. Activity Report 2015. CEMBUREAU, Brussels, Belgium.

Damidot D, Lothenbach B, Herfort D, et al., 2011. Thermodynamics and cement science. *Cement and Concrete Research*, 41(7):679-695. https://doi.org/10.1016/j.cemconres.2011.03.018

Damtoft JS, Lukasik J, Herfort D, et al., 2008. Sustainable development and climate change initiatives. *Cement and Concrete Research*, 38(2):115-127. https://doi.org/10.1016/j.cemconres.2007.09.008

Dhandapani Y, Sakthivel T, Santhanam M, et al., 2018. Mechanical properties and durability performance of concretes with limestone calcined clay cement (LC^3). *Cement and Concrete Research*, 107:136-151. https://doi.org/10.1016/j.cemconres.2018.02.005

Díaz YC, Berriel SS, Heierli U, et al., 2017. Limestone calcined clay cement as a low-carbon solution to meet expanding cement demand in emerging economies. *Development Engineering*, 2:82-91. https://doi.org/10.1016/j.deveng.2017.06.001

Edenhofer O, Pichs-Madruga R, Sokona Y, et al., 2014. Climate Change 2014: Mitigation of Climate Change. Contribution of Working Group III to the Fifth Assessment Report of the Intergovernmental Panel on Climate Change. Cambridge University Press, Cambridge, UK.

GAQSIQ (General Administration of Quality Supervision and Quarantine), SA (Standardization Administration), 2005. Test Method for Fluidity of Cement Mortar, GB/T 2419-2005. National Standards of the People's Republic of China (in Chinese).

GAQSIQ (General Administration of Quality Supervision and Quarantine), SA (Standardization Administration), 2007. Common Portland Cement, GB 175-2007. National Standards of the People's Republic of China (in Chinese).

Gmür R, Thienel KC, Beuntner N, 2016. Influence of aging conditions upon the properties of calcined clay and its performance as supplementary cementitious material. *Cement and Concrete Composites*, 72:114-124. https://doi.org/10.1016/j.cemconcomp.2016.05.020

Hou LJ, Zhou BX, Guo S, et al., 2018. Bond-slip behavior between pre-corroded rebar and steel fiber reinforced concrete. *Construction and Building Materials*, 182:637-645. https://doi.org/10.1016/j.conbuildmat.2018.06.116

Kelly TD, Matos GR, 2015. Historical Statistics for Mineral and Material Commodities in the United States. U.S. Geological Survey, USA. http://minerals.usgs.gov/minerals/pubs/historical-statistics

Liao WY, Kumar A, Khayat K, et al., 2019. Multifunctional lightweight aggregate containing phase change material and water for damage mitigation of concrete. *ES Materials & Manufacturing*, 6:49-61. https://doi.org/10.30919/esmm5f606

Lothenbach B, Le Saout G, Gallucci E, et al., 2008. Influence of limestone on the hydration of Portland cements. *Cement and Concrete Research*, 38(6):848-860. https://doi.org/10.1016/j.cemconres.2008.01.002

Lothenbach B, Scrivener K, Hooton RD, 2011. Supplementary cementitious materials. *Cement and Concrete Research*, 41(12):1244-1256. https://doi.org/10.1016/j.cemconres.2010.12.001

Ma HY, 2014. Mercury intrusion porosimetry in concrete technology: tips in measurement, pore structure parameter acquisition and application. *Journal of Porous Materials*, 21(2):207-215. https://doi.org/10.1007/s10934-013-9765-4

Ma HY, Li ZJ, 2013a. Realistic pore structure of Portland cement paste: experimental study and numerical simulation. *Computers and Concrete*, 11(4):317-336. https://doi.org/10.12989/cac.2013.11.4.317

Ma HY, Li ZJ, 2013b. Microstructures and mechanical properties of polymer modified mortars under distinct mechanisms. *Construction and Building Materials*, 47:579-587. https://doi.org/10.1016/j.conbuildmat.2013.05.048

Ma HY, Hou DS, Li ZJ, 2015. Two-scale modeling of transport properties of cement paste: formation factor, electrical conductivity and chloride diffusivity. *Computational Materials Science*, 110:270-280. https://doi.org/10.1016/j.commatsci.2015.08.048

Martirena F, Favier A, Scrivener K, 2018. Calcined Clays for Sustainable Concrete. Springer, Dordrecht, the Netherlands. https://doi.org/10.1007/978-94-024-1207-9

Matschei T, Lothenbach B, Glasser FP, 2007. The role of calcium carbonate in cement hydration. *Cement and Concrete Research*, 37(4):551-558. https://doi.org/10.1016/j.cemconres.2006.10.013

MHURC (Ministry of Housing and Urban-Rural Construction), 2011. Specification for Mix Proportion Design of Ordinary Concrete, JGJ 55-2011. National Standards of the People's Republic of China (in Chinese).

Muzenda TR, Hou PK, Kawashima S, et al., 2020. The role of limestone and calcined clay on the rheological properties of LC3. *Cement and Concrete Composites*, 107:103516. https://doi.org/10.1016/j.cemconcomp.2020.103516

Nidheesh PV, Kumar MS, 2019. An overview of environmental sustainability in cement and steel production. *Journal of Cleaner Production*, 231:856-871. https://doi.org/10.1016/j.jclepro.2019.05.251

SBQTS (State Bureau of Quality and Technical Supervision), 1999. Method of Testing Cements–Determination of Strength, GB/T 17671-1999. National Standards of the People's Republic of China (in Chinese).

Schneider M, Romer M, Tschudin M, et al., 2011. Sustainable cement production—present and future. *Cement and Concrete Research*, 41(7):642-650. https://doi.org/10.1016/j.cemconres.2011.03.019

Scrivener K, Favier A, 2015. Calcined Clays for Sustainable Concrete. Springer, Dordrecht, the Netherlands. https://doi.org/10.1007/978-94-017-9939-3

Scrivener K, John V, Gartner E, 2018a. Eco-efficient cements: potential economically viable solutions for a low-CO_2 cement-based materials industry. *Cement and Concrete Research*, 114:2-26. https://doi.org/10.1016/j.cemconres.2018.03.015

Scrivener K, Martirena F, Bishnoi S, et al., 2018b. Calcined clay limestone cements (LC^3). *Cement and Concrete Research*, 114:49-56. https://doi.org/10.1016/j.cemconres.2017.08.017

Ston J, Scrivener K, 2019. Basic creep of limestone–calcined clay cements: an experimental and numerical approach. *Theoretical and Applied Fracture Mechanics*, 103:102270. https://doi.org/10.1016/j.tafmec.2019.102270

Tironi A, Trezza MA, Scian AN, et al., 2012a. Incorporation of calcined clays in mortars: porous structure and compressive strength. *Procedia Materials Science*, 1:366-373. https://doi.org/10.1016/j.mspro.2012.06.049

Tironi A, Trezza MA, Scian AN, et al., 2012b. Kaolinitic calcined clays: factors affecting its performance as pozzolans. *Construction and Building Materials*, 28(1):276-281. https://doi.org/10.1016/j.conbuildmat.2011.08.064

Wang L, Shen N, Zhang MM, et al., 2020. Bond performance of steel-CFRP bar reinforced coral concrete beams. *Construction and Building Materials*, 245:118456. https://doi.org/10.1016/j.conbuildmat.2020.118456

Zhou YW, Fu HK, Li PD, et al., 2019. Bond behavior between steel bar and engineered cementitious composite (ECC)

considering lateral FRP confinement: test and modeling. *Composite Structures*, 226:111206. https://doi.org/10.1016/j.compstruct.2019.111206

中文概要

题　目：华南地区煅烧粘土−石灰石复合水泥（LC^3）混凝土的研发及其与钢筋的粘结性能

目　的：采用华南地区的原材料研发一种 LC^3 水泥胶凝材料，并研究其水化反应、微观结构的发展、工作性能、强度性能的发展以及混凝土和钢筋之间的粘结-滑移行为，为推广 LC^3 水泥胶凝材料应用于滨海结构混凝土提供基础信息和参考。

创新点：1. 鉴于目前对 LC^3 水泥胶凝材料在混凝土技术和结构混凝土中的应用研究较少，本文对采用华南地区原材料制备的 LC^3 混凝土进行了技术研究和应用分析；2. 试验结果发现，LC^3 混凝土的抗折和劈裂性能优于相同抗压强度的普通混凝土；3. 采用拔出试验研究 LC^3 混凝土与钢筋之间的界面粘结-滑移行为，证明了新型 LC^3 水泥胶凝材料在钢筋混凝土结构中的适用性。

方　法：1. 开展一系列基于 LC^3 水泥的净浆、砂浆和混凝土的实验研究，并使用原始材料进行微观结构分析（水化产物表征和孔结构分析）和宏观测试（工作性能和力学性能测试）。2. 研究 LC^3 混凝土与钢筋之间的粘结-滑移行为。

结　论：1. 与普通混凝土（OPC）相比，钙矾石、单碳铝酸盐（MC）和半碳铝酸盐（HC）是 LC^3 样品中的主要晶体水合产物；由于熟料减少 50%，且 LC^3 中发生的二次水化反应消耗了大量 OPC 熟料水化生成的氢氧化钙（CH），因此在 LC^3 的水合产物中几乎没有残留六角形薄片 CH。2. 与 OPC 砂浆和混凝土相比，LC^3 砂浆和混凝土的早期强度较低；由于在煅烧粘土中无定形二氧化硅和氧化铝（与石灰石结合）二次反应形成了更多的水化硅酸钙和碳铝酸钙水合物，LC^3 砂浆和混凝土的后期强度（7 天后）迅速增加至与 OPC 砂浆和混凝土相当的强度水平。3. 在与 OPC 同类材料具有相同抗压强度的情况下，LC^3 水泥胶凝材料具有更高的抗折和劈裂强度，因此更有韧性。4. 对于 LC^3 水泥胶凝材料，颗粒更细的石灰石不一定会带来更好的力学性能。5. 对于混凝土与钢筋之间的界面粘结-滑移行为，LC^3 的破坏模式与 OPC 大致相同，且通常有两种破坏模式，即钢筋从混凝土中拔出和混凝土劈裂破坏；在具有相同等级的抗压强度时，LC^3 混凝土的粘结强度与 OPC 混凝土相当，但其粘结-滑移刚度更大。

关键词：煅烧粘土-石灰石复合水泥；水化反应；粘结-滑移；压汞孔隙度测定法；扫描电子显微镜；粘结强度